Dysobinol from *Chisocheton macrophyllus* Selectively Induces G1 Cell Cycle Arrest in MCF-7 Breast Cancer Cells

Shabarni Gaffar[1*], Ghina Uli Felicia Tambunan[1], Ersanda Hafiz[1], Tati Herlina[1], Hesti Lina Wiraswati[2], Nurlelasari Nurlelasari[1], and Ilma Fauziah Ma'ruf[3]

[1]*Department of Chemistry, Faculty of Mathematics and Natural Sciences, Universitas Padjadjaran, Jl. Raya Bandung-Sumedang Km. 21, Jatinangor, Sumedang 45363, Indonesia*

[2]*Department of Biomedical Sciences, Faculty of Medicine, Universitas Padjadjaran, Jl. Raya Bandung-Sumedang Km. 21, Jatinangor, Sumedang 45363, Indonesia*

[3]*Research Center for Climate and Atmosphere, National Research and Innovation Agency, Jl. Sangkuriang, Bandung 40135, Indonesia*

**** Corresponding author:***

email: shabarni.gaffar@unpad.ac.id

Received: October 7, 2024
Accepted: September 11, 2025

DOI: 10.22146/ijc.100479

Abstract: Chisocheton macrophyllus *is a medicinal plant that contains sesquiterpenoids, triterpenoids, limonoids, steroids, and phenolic compounds. This research aimed to assess the effect of Dysobinol, a limonoid compound from the seed of* C. macrophyllus*, on MCF-7 cell growth. Cell viability was evaluated using the MTS colorimetric assay, DNA fragmentation was assessed by agarose electrophoresis, apoptosis and cell cycle arrest were determined by flow cytometry, and gene expression levels were evaluated using qRT-PCR. Dysobinol was also analyzed* in silico *using drug-likeness, pharmacokinetic, and molecular docking analysis. Dysobinol demonstrated moderate cytotoxicity against MCF-7 cells, with an* IC_{50} *of 148.20 µg/mL. Dysobinol induced G1 phase cell cycle arrest that was not accompanied by the induction of apoptosis in MCF-7 cells.* In silico *studies showed that the EGFR/AKT/cyclin D1 proteins were affected by Dysobinol. Furthermore, drug-likeness and pharmacokinetics analysis showed that Dysobinol is bioavailable orally and has high gastrointestinal absorption and low penetration into the blood-brain barrier. Together, these results indicate that Dysobinol can regulate breast cancer cell proliferation through cell cycle arrest rather than apoptosis, and its pharmacological profile highlights its potential as a promising lead compound for anticancer drug development.*

Keywords: *cell cycle arrest; Dysobinol; DNA fragmentation; molecular docking; pharmacokinetics*

■ INTRODUCTION

Cancer is the second leading cause of death around the globe, where cervical and breast cancer are among the most significant contributors to the cause of death for women [1]. The search for new candidates for cancer treatment is one of the efforts to overcome treatment limitations, including cases of resistance and side effects from chemotherapy drugs. Plants are one source of drugs that are believed to be able to be used to obtain new drugs; therefore, many studies have been conducted *in silico*, *in vitro*, and *in vivo* on medicinal plants [2-4]. The National Cancer Institute (NCI) reports that 35,000 plant species have been researched, with 3,000 identified as having potential anticancer properties [5]. Plant phytochemicals have been reported to have various anticancer effects, such as inhibiting cell proliferation and cell cycle arrest or inducing cancer cell death [6-7]. Paclitaxel is an example of an alkaloid plant-derived chemical agent in clinical use [8]. Saponins, quinones, flavonoids, tannins, and terpenoids are other phytochemical groups reported to have anticancer effects [9-12].

Chisocheton is a genus of the *Meliaceae* family consisting of 50 species distributed in India, Vietnam,

Myanmar, Brunei, the Philippines, China, Thailand, Indonesia, Malaysia, and Papua New Guinea. The *Chisocheton* genus is known to contain various compounds, including limonoids, tirucallane, dammarane, lupane, oleanane, steroids, sesquiterpenes, anthraquinones, alkaloids, coumarins, and simple phenolics [13]. Limonoids are oxygenated triterpenoid derivatives that have lost four terminal carbon atoms in their side chains, forming a furan ring [14-15]. These compounds are commonly found in the genus *Chisocheton*. Limonoids have been reported to possess various biological activities, such as anticancer [16-18], antiplasmodial [19], antimicrobials [20], apoptosis-inducing [21], antivirals [22], anti-inflammatories [23-25], antiobesity [26], insecticidal [27], and antifungal activities [28].

Several studies have reported the anticancer activity of limonoid compounds against cancer cells. Limonoids from the seeds of *C. macrophyllus*, namely, Dysobinol, 7α-hydroxyneotrisilinone, dysobinin, and nimonol, exhibited cytotoxic effects on P388 cells, with IC_{50} values of 19.5, 64.5, 49.7, and 79.4 μg/mL, respectively [29]. Dysobinin, azadiradione, mahonin, and epoxiazadiradione from the seeds of *C. siamensis* have been reported to have anticancer effects on MCF-7 cells, with IC_{50} values of 2.15, 7.13, 18.42, and 4.68 μg/mL, respectively [30]. Ceramicin G and ceramicin I, which are compounds from the stem of *C. ceramicus*, were found to have anticancer effects on HL-60 and MCF-7 cells, with IC_{50} values of 11.85 and 12.39 μg/mL (ceramicin G) and 19.71 and 20.42 μg/mL (ceramicin I) [31]. The limonoid compounds pentandricin, ceramicin B, 6-de(acetoxy)-23-oxochisocheton, and 6-de(acetoxy)-23-oxo-7-*O*-deacetylchisocheton from the bark of *C. pentandrus* exhibited cytotoxic effects on MCF-7 cells, with IC_{50} values of 162.73, 61.55, 94.44, and 49.24 μg/mL, respectively [32]. Limonoids have been reported to exhibit anticancer activity against various cancer cell lines, including leukemia cells (MOLT-4 and P388) [33], colorectal cancer cells [34], breast cancer cells (MCF-7) [35], liver cancer cells (HepG2) [36], and neuroblastoma cells [37]. Moreover, they have also been shown to inhibit the growth of breast cancer cells that express estrogen receptors (ER^+) as well as those that do not express estrogen receptors (ER^-) [38].

Breast cancer is the second most common cancer, following cervical cancer, and is expected to become the most widespread cancer among women. Breast cancer typically develops in the epithelial tissue of the breast, where it continues to grow and eventually forms a lump. Breast cancer occurs almost exclusively in women (99%) but can also occur in men (1%) [39]. Approximately 90% of breast cancer cases occur in Western countries and developed Asian countries [40].

Previous research demonstrated the anticancer activity of Dysobinol against P388 cells, with an IC_{50} of 19.5 μg/mL [29]. This study is the first to investigate the cytotoxic effects and underlying mechanisms of this compound in MCF-7 breast cancer cells. The cytotoxicity of Dysobinol was evaluated alongside its ability to induce apoptosis and disrupt the cell cycle, using DNA fragmentation assays, apoptotic cell quantification, and flow cytometric analysis. These findings provide insight into the mechanism of action of Dysobinol and support its potential as a lead compound for the development of breast cancer drugs.

■ EXPERIMENTAL SECTION

Materials

The MCF-7 cell line was obtained from the Central Laboratory of Padjadjaran University. Dysobinol (Colorless crystal, m.p. 194–195 °C, IR (KBr, max, cm^{-1}): 3448, 1755, 1743, 1680, 1606. HR-ESI-TOF/MS *m/z* 551.2287 $[M+Na]^+$ (calcd for $C_{30}H_{40}O_8Na$, 551.3343), was provided by Nurlelasari et al. [29]. An apoptotic DNA ladder kit was obtained from Roche, and a FITC Annexin V Apoptosis Detection Kit with propidium iodide (PI) was purchased from BD Biosciences. Roswell Park Memorial Institute-1640 (RPMI-1640) medium, fetal bovine serum (FBS), penicillin, streptomycin sulfate, trypsin-EDTA, and trypan blue dye were purchased from Gibco. An MTS assay kit (CellTiter 96® Aqueous One Solution Cell Proliferation Assay Kit) was purchased from Promega. TRIsure™ was from Meridian-Bioscience, and the SensiFAST™ SYBR® No-ROX One-Step Kit was from Bioline. Other chemicals, such as DMSO, SDS, chloroform, isopropyl alcohol, ethanol, DEPC-treated water, agarose, diamond nucleic acid gel stain, loading

dye, TAE buffer (Tris-acetic acid-EDTA), ethanol, isopropanol, PBS, and nuclease-free water (NFW), were of cell culture grade and were purchased from Sigma-Aldrich.

Instrumentation

All experiments were conducted using standard cell culture facilities, including a CO_2 incubator (Thermo Fisher Scientific, USA) and a Class II biosafety cabinet (Esco, Singapore). Cell viability was assessed in 96-well microplates (Corning, USA) and absorbance was measured with a multimode microplate reader (NanoQuant, TECAN, Switzerland). The DNA fragment was separated by agarose gel electrophoresis in a horizontal electrophoresis apparatus (Bio-Rad, USA), with DNA bands visualized under a UV transilluminator (Bio-Rad Gel Doc, USA). Apoptosis and cell cycle were analyzed by flow cytometry (BD FACS-Calibur, USA) equipped with CellQuest software (version 2.5.1, BD Biosciences, USA), and data were further processed using Flowing Software (version 2.5.1, Turku Centre for Biotechnology, Finland) and Microsoft Excel 2013 (Microsoft Corp., USA). Total RNA was quantified using the NanoQuant multimode instrument (TECAN, Switzerland), and quantitative RT-PCR was done on the ARIA MX Real-Time PCR system (Agilent Technologies, USA).

Procedure

Cytotoxic activity assay

MCF-7 cells were cultured in RPMI medium supplemented with 10% FBS, 100 U/mL penicillin, and 100 µg/mL streptomycin, and maintained for 24 h until reaching approximately 80% confluence. Cells were then harvested, counted, and seeded into a 96-well plate at a density of 1.7×10^4 cells/well, followed by a 24-h incubation. The culture medium was subsequently replaced, and the cells were exposed for another 24 h to varying concentrations of Dysobinol (1.95–250 µg/mL) prepared in 10% (v/v) DMSO in PBS, with the final solvent concentration maintained below 0.2% to avoid cytotoxic effects or color interference. Doxorubicin (0.75–48 µg/mL) served as a positive control. After treatment, 20 µL of MTS reagent was added to each well and incubated for 4 h at 37 °C. The reaction was stopped by adding 10% SDS, and absorbance was recorded at 490 nm using a microplate reader (NanoQuant, TECAN).

Observation of DNA fragmentation

MCF-7 cells (1.8×10^6 cells/well) were seeded in a 12-well plate and incubated for 24 h. The medium was then replaced, and cells were treated for 24 h with Dysobinol (50, 100, or 200 µg/mL). Untreated and DMSO-treated cells served as controls. DNA was extracted using an apoptotic DNA ladder kit, dissolved in nuclease-free water, and analyzed by agarose gel electrophoresis (1.5 h, 80 V) with UV visualization.

Determination of apoptosis by Annexin V-FITC/PI flow cytometry

MCF-7 cells (0.3×10^6 cells/well) were seeded in 6 cm petri dishes and incubated for 24 h, The medium was then replaced and treated for a further 24 h with Dysobinol (50, 100, or 200 µg/mL). Following treatment, cells were harvested with 0.25% trypsin-EDTA, centrifuged at 2000 rpm for 3 min, washed twice with PBS, and kept on ice. The pellet was further washed twice with cell staining buffer, resuspended in 100 µL Annexin V binding buffer, and transferred to flow cytometry tubes. Annexin V-FITC (5 µL) and PI (10 µL) were added, and samples were vortexed and incubated for 15 min at room temperature (25 °C) in the dark. Afterward, 400 µL Annexin V binding buffer was added, and the samples were analyzed by a flow cytometer (FAC-Scan v2.5.1) data were processed with Microsoft Excel 2013.

Cell cycle arrest analysis by flow cytometry

MCF-7 cells were seeded in 6 cm petri dishes following the same procedure used for apoptosis determination. Cells were harvested by adding 0.25% trypsin-EDTA and centrifuging at 2000 rpm for 3 min. The cell pellet was washed twice with cold PBS. Cells were resuspended in 400 µL of PI, and 1 mL of DEPC-treated water. The mixture was incubated for 10 min at 37 °C. DNA content was analyzed using flow cytometry and Flowing software (version 2.5.1), as well as Excel in Microsoft Office 2013.

RNA isolation and determination of gene expression levels by qRT-PCR

MCF-7 cells (1.8×10^6 cells/well) were seeded in a 12-well plate, incubated for 24 h following the previous procedure, and treated for a further 24 h with Dysobinol

(100 and 200 µg/mL). Total RNA was extracted using TRI-sure™ reagent according to the manufacturer's protocol, and the concentration was measured using a multimode reader instrument. Quantitative PCR was performed using the One-Step SensiFAST™ SYBR® NO-ROX kit using 5 ng/µL of RNA template per reaction following the instructions of the ARIA MX real-time qRT-PCR instrument. The PCR procedure consisted of two steps: the first step involved reverse transcription at 45 °C for 10 min, and the second step involved PCR cycling, which consisted of an initial denaturation at 95 °C for 2 min, followed by 40 cycles of denaturation at 95 °C for 5 s and annealing/extension at 60 °C for 20 s. Primers were designed based on the gene sequences available in NCBI (Table 1). Gene expression was quantified using the $2^{-\Delta\Delta C_T}$ method, with β-actin as the reference housekeeping gene [41].

Statistical analysis

The data presented are the averages of three experiments. The qPCR results were analyzed using Minitab version 17, and ANOVA was conducted at a 95% confidence level. Differences were considered statistically significant if the *p*-value was less than 0.05. Tukey's post hoc test was used to compare the means of each treatment with the means of all the other treatments.

Drug-likeness and pharmacokinetic analysis

The SwissADME (http://www.swissadme.ch/) was used to analyze the likeness and pharmacokinetics of Dysobinol and compare it with dysobinin. The drug-likeness analysis was performed according to the criteria of Lipinski, Ghose, Veber, Egan, and Muegge [42].

Molecular docking analysis

The crystal structures of the proteins used for molecular docking analysis were downloaded from the Protein Data Bank (https://www.rcsb.org/). The protein was separated from its native ligand to provide a pocket for molecular docking. Molecular docking analysis was attempted using AutoDock Vina [43] and UCSF Chimera [44]. Native ligand docking was performed for docking validation. For a specific docking approach, the gridbox was set as follows: EGFR (center_x = 31.935, center_y = -16.447, center_z = 3.567, size_x = 24, size_y = 10, size_z = 16), VEGFR1 (center_x = 5.377, center_y = 18.452, center_z = 31.774, size_x = 18, size_y = 14, size_z = 16), VEGFR2 (center_x = 20.194, center_y = 25.385, center_z = 37.986, size_x = 20, size_y = 12, size_z = 14), mutant HER alpha ligand binding domain (center_x = -2.00, center_y = 52.00, center_z = 164.00, size_x = 15.00, size_y = 15.00, size_z = 15.00), estrogen receptor alpha rbd (center_x = 67.00, center_y = 35.00, center_z = 18.00, size_x = 20.00, size_y = 20.00, size_z = 20.00), estrogen receptor α ligand-binding domain (center_x = −15.00, center_y = 1.00, center_z = -27.00, size_x = 20.00, size_y = 20.00, size_z = 20.00), AKT (center_x = −20.00, center_y = 5.00, center_z = 11.00, size_x = 17.00, size_y = 17.00, size_z = 17.00) and CDK6 (center_x = 15.00, center_y = 27.00, center_z = 10.00, size_x = 17.00, size_y = 17.00, size_z = 17.00). UCSF Chimera and Ligplot Plus were used for molecular docking visualization [45].

■ RESULTS AND DISCUSSION

Cytotoxic Effect of Dysobinol on MCF-7 Cells

The viability of MCF-7 cells decreased in a concentration-dependent manner after treatment with Dysobinol, yielding an IC_{50} of 148.20 µg/mL, whereas doxorubicin showed much greater potency with an IC_{50} of 15.55 µg/mL (Fig. 1). Morphologically, untreated MCF-7 cells formed thin, oval, adherent monolayers,

Table 1. Sequences of primers used in this study

Gene	Forward primer	Reverse primer
p53	5'-CCTCAGCATCTTATCCGAG-3'	5'-TGGATGGTGGTACAGTCAG-3'
Bcl-2	5'-CAGGCCGGCGACGACTTCTC-3'	5'-TCCCGGTTGACGCTCTCCAC-3'
CycD1	5-'AGGCGGAGGAGAACAAACAC-3'	5'-GTGAGGCGGTAGTAGGACAG-3'
NF_KB	5'-CAAGGCAGCAAATAGACGAG-3'	5'-GGGCATTTTGTTGAGAGTTAG-3'
B-act	5'-GATCATTGCTCCTCCTGAGC-3'	5'-TAGAAGCATTTGCGGTGGAC-3'

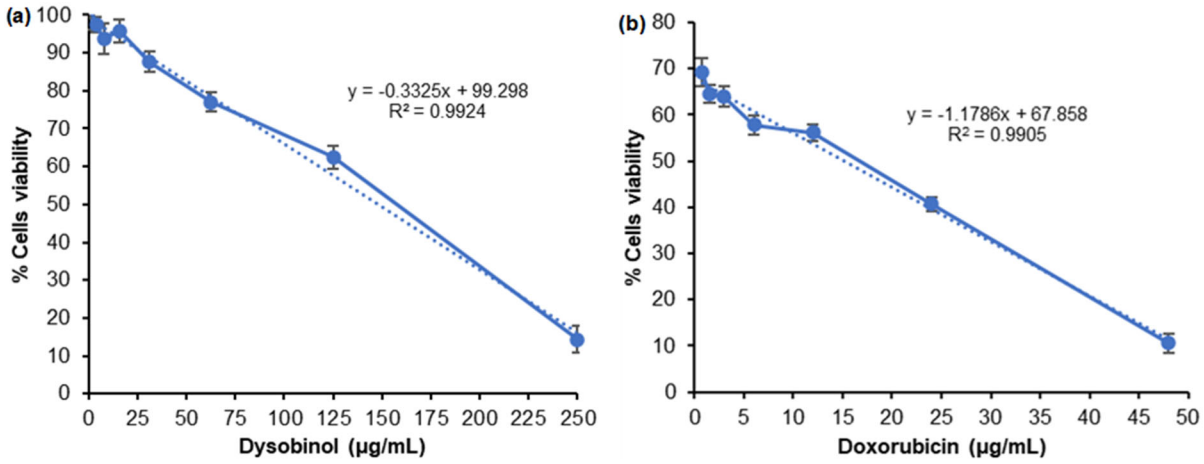

Fig 1. Viability of MCF-7 cells after treatment with (a) Dysobinol and (b) doxorubicin for 24 h. Data represent the mean ± SD of the three independent experiments

while Dysobinol-treated cells appeared rounded and detached from the culture surface (data not shown). Based on US NCI criteria, Dysobinol is classified as moderately cytotoxic (21–200 µg/mL), whereas doxorubicin falls into the highly cytotoxic category (< 20 µg/mL) [46].

Dysobinol Affects Cell Cycle Arrest in MCF-7 Cells

Table 2 summarizes the distribution of MCF-7 cells across cell cycle phases after 24 h of treatment with Dysobinol (50, 100, and 200 µg/mL). Dysobinol induced a concentration-dependent accumulation of cells in the G1 phase, accompanied by a slight increase in the sub-G1 population, while the proportions of cells in the S and G2/M phases decreased relative to controls. These changes indicate that Dysobinol inhibits progression beyond the G1 checkpoint, thereby reducing DNA replication and limiting entry into G2/M. The DNA content in the G1 phase (Fig. 2) increased following Dysobinol treatment, indicating cell cycle arrest at this checkpoint and a consequent reduction in MCF-7 cells entering the S phase. Targeting the G1 phase has been a key strategy in anticancer drug development, with several agents evaluated *in silico*, *in vitro*, and *in vivo*, and some progressing to clinical trials for breast cancer [47].

Dysobinol Does Not Induce Apoptosis in MCF-7 Cells

To monitor whether cell cycle arrest was accompanied by apoptosis in MCF-7 cells, cells positive for PI/Annexin V were analyzed by flow cytometry (Fig. 3).

Table 2. The percentage of DNA in each cell cycle phase was determined in control cells and MCF-7 cells treated with Dysobinol for 24 h by flow cytometry combined with PI staining

Treatment	DNA populations (%)			
	Sub-G1	G1	S	G2/M
Control cells	1.5	27.4	26.9	43.6
50 µg/mL Dysobinol	2.9	36.7	28.3	31.2
100 µg/mL Dysobinol	3.2	41.1	25.4	29.4
200 µg/mL Dysobinol	5.5	51.1	19.4	23.5

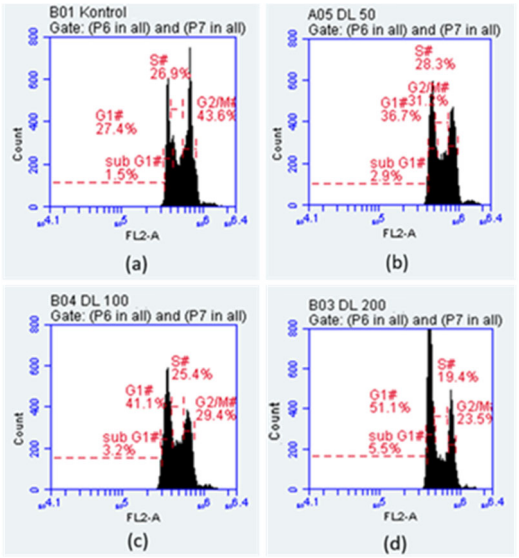

Fig 2. DNA population profiles at each phase of the cell cycle in (a) control cells and MCF-7 cells treated with (b) 50 µg/mL, (c) 100 µg/mL, or (d) 200 µg/mL Dysobinol, determined by flow cytometry with PI staining

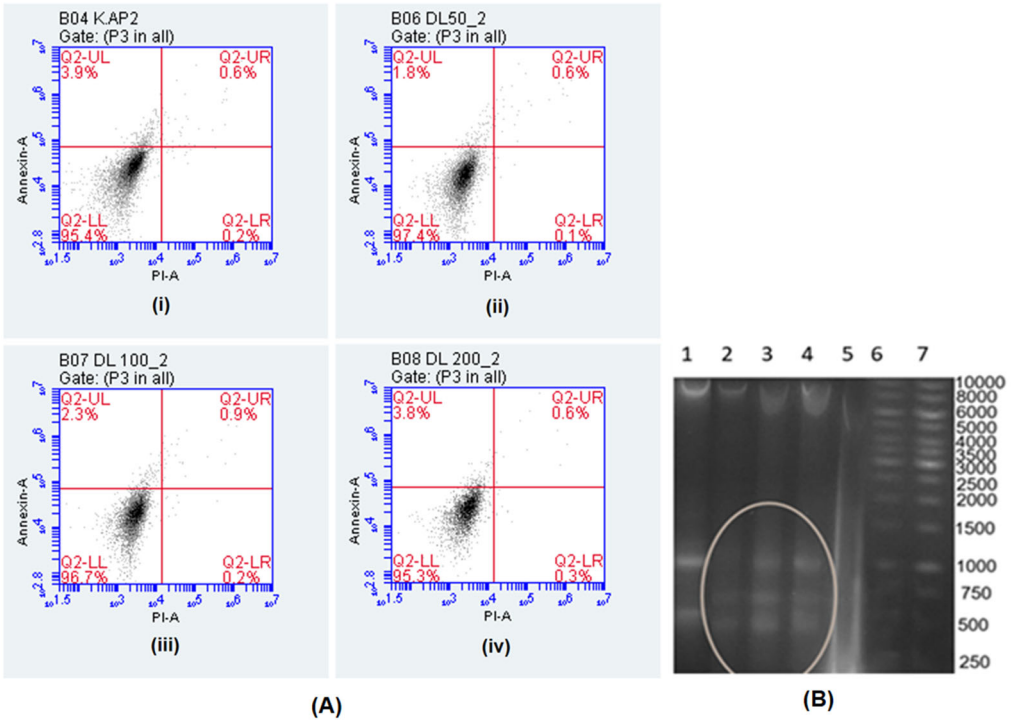

Fig 3. The effect of Dysobinol on MCF-7 cell death; (a) MCF-7 cells were treated with Dysobinol for 24 h and quantified by flow cytometry to determine PI uptake (PI positivity) and exposure to phosphatidyl serine (Annexin V positivity); (i) medium (control), (ii) 50 µg/mL Dysobinol, (iii) 100 µg/mL Dysobinol, and (iv) 200 µg/mL Dysobinol. (b) The DNA fragmentation pattern of MCF7 cells characterized by agarose gel electrophoresis. (1) DMSO, (2) 50 µg/mL Dysobinol, (3) 100 µg/mL Dysobinol, (4) 200 µg/mL Dysobinol, (5) doxorubicin, and (6, 7) 1 kb DNA ladder

This assay aims to observe phosphatidyl serine exposure on the outer membrane during apoptosis, which binds to Annexin V. PI will specifically stain cells by intercalating into DNA [48]. The results showed that cells did not undergo apoptosis (at the same concentration and duration as those used in the cell cycle experiment). Most cells were PI-negative and Annexin V-negative (95–98%). These findings are consistent with our observations of DNA fragmentation (one of the biochemical markers of apoptosis), where complete DNA fragmentation (a DNA ladder) does not occur.

The Gene Expression Level of MCF-7 Cells Treated with Dysobinol

The results of the quantitative PCR analysis of several carcinogenesis genes indicated that treatment of MCF-7 cells with 100 or 200 µg/mL Dysobinol significantly altered the expression of the cyclin D1 and Bcl-2 genes (Fig. 4). A one-way ANOVA followed by the Tukey post hoc test revealed significant changes in the expression of Bcl-2 (3.01× and 4.22×) and Cyc D1 (−0.47× and −0.36×) in MCF7 cells treated with Dysobinol. Furthermore, the change in NF_KB gene expression reached significance only at higher doses. However, there were no significant changes in the expression of the transcription factor p53. These qPCR results are consistent with the observed inhibition of the cell cycle, indicating G1 phase arrest, which was confirmed by decreased expression of Cyclin D1. The significant increase in Bcl-2 expression after treatment with Dysobinol suggested that this compound does not induce apoptosis, as shown by flow cytometry results.

Drug-Likeness and Pharmacokinetic Analysis

The drug-likeness analysis (Table 3) showed that Dysobinol meets all five drug-likeness criteria (Lipinski, Ghose, Veber, Egan, Muegge). The ADME analysis suggests that Dysobinol has more favorable drug-like

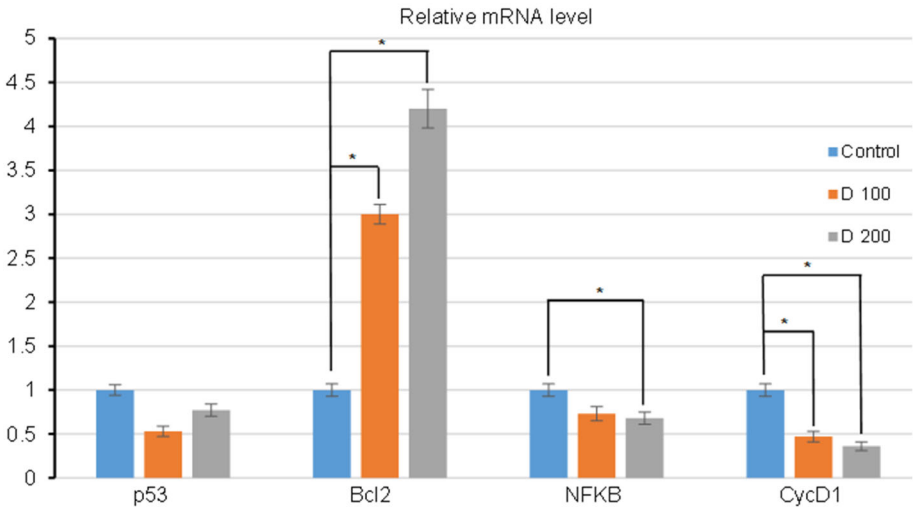

Fig 4. Expression levels of the p53, Bcl-2, Cyc D1, and NF_KB genes after administration of Dysobinol to MCF7 cells for 24 h. Blue = control cells (without treatment), orange = Dysobinol (100 µg/mL), gray = Dysobinol (200 µg/mL). Gene expression was normalized to that of β-actin. Data are presented as mean ± SD and are representative of three experiments. Bars that do not share a letter differ significantly for each gene based on one-way ANOVA, followed by the Tukey post hoc test with a significance level of a = 0.05

Table 3. The drug-likeness analysis

Parameter	Dysobinol	Dysobinin
MW	470.10	494.62
Hydrogen-Bond:		
Acceptors	8	6
Donor	2	0
Fraction Csp	0.65	0.63
Rotatable bond	5	5
MR	118.19	136.18
TPSA	123.27	82.81
Consensus log-P	1.98	4.74
ESOL log-S	−3.44	−6.03
ESOL Class	Soluble	Poorly Soluble
Violation:		
Lipinski	0	0
Ghose	0	4
Veber	0	0
Egan	0	0
Muegge	0	1

properties compared to dysobinin. Dysobinol complies fully with Lipinski, Ghose, Veber, Egan, and Muegge rules, indicating strong drug-likeness with no violations. It also exhibits better solubility (ESOL log-S = −3.44, classified as soluble) and acceptable lipophilicity (consensus log P = 1.98), which supports good oral bioavailability. In contrast, dysobinin exhibits multiple violations (Ghose, Veber, Muegge), higher lipophilicity (log P = 4.74), and poor solubility (ESOL log-S = −6.03), which may limit its bioavailability. Moreover, the higher topological polar surface area (TPSA = 123.27 $Å^2$) and hydrogen bond donors/acceptors in Dysobinol suggest a stronger potential for biological interactions without compromising permeability. Overall, Dysobinol is predicted to be a more promising orally bioavailable and synthetically accessible lead compound compared to dysobinin.

The pharmacokinetic analysis further supports the potential of Dysobinol as a drug candidate. Both Dysobinol and dysobinin showed comparable bioavailability scores (0.55) and high gastrointestinal (GI) absorption, but neither compound was predicted to cross the blood–brain barrier (BBB), which is desirable for minimizing central nervous system side effects. Importantly, Dysobinol exhibited fewer structural alerts (one Brenk alert and one lead-likeness violation) compared to dysobinin, which had two Brenk alerts and two lead-likeness violations. In addition, Dysobinol demonstrated slightly better synthetic accessibility (6.58) than dysobinin (6.25), indicating it remains feasible for chemical synthesis (Table 4). Overall, these findings suggest that

Table 4. Pharmacokinetic analysis of Dysobinol and dysobinin

Compounds	Bioavailability score	GI Absorption	BBB Permeant	Alerts		Lead-likeness violation	Synthetic accessibility
				PAINS	BRENK		
Dysobinol	0.55	High	No	0	1	1	6.58
Dysobinin	0.55	High	No	0	2	2	6.25

Dysobinol has a more favorable pharmacokinetic and safety profile than dysobinin, reinforcing its potential as a lead compound of natural origin.

Molecular Docking Analysis

To investigate the molecular mechanism underlying G1 arrest in MCF-7 cells induced by Dysobinol, molecular docking was performed against key receptor proteins, including EGFR, VEGFR1, VEGFR2, the HERα and ERα ligand-binding domains, AKT, and CDK6. Molecular docking analysis revealed that Dysobinol interacted with several cancer-related protein targets, although with generally lower affinity than the native ligands (Table 5, Fig. 5–10). Dysobinol showed the strongest binding

Table 5. Binding affinity results in the specific docking to particular proteins compared to native ligands

Protein target	Docking score (kcal/mol)		
	Native ligand	Dysobinol	Dysobinin
EGFR (7LGS)	−8.5	−6.3	−6.6
VEGFR-1 (3HNG)	−10.9	2.0	4.8
VEGFR-2 (4AG8)	−11.1	−2.4	0.8
Mutant ERα (1QKT)	−10.6	−7.1	−5.6
Erα rbd (2YAT)	−9.4	−5.6	−5.4
ERα ligand-binding domain (2JF9)	−10.1	−4.9	−4.5
AKT (4GV1)	−9.4	−8.2	−8.2
CDK6 (5L21)	−11.1	−5.6	−5.0

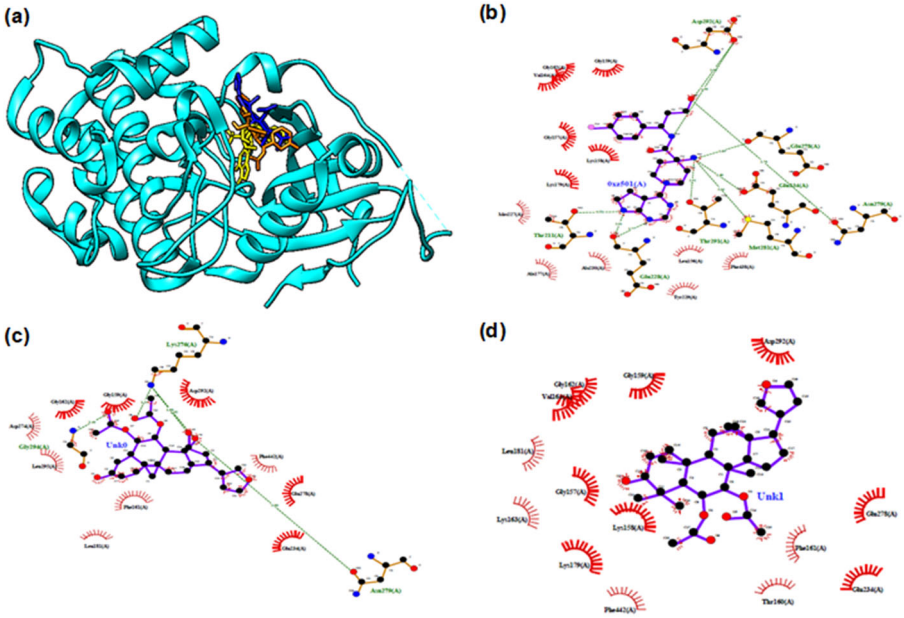

Fig 5. Binding visualization of ligand on AKT: (a) 3-dimensional visualization of native ligand (yellow), Dysobinol (orange) and dysobinin (blue), (b) native ligand interaction with AKT, (c) Dysobinol interaction with AKT, and (d) dysobinin interaction with AKT

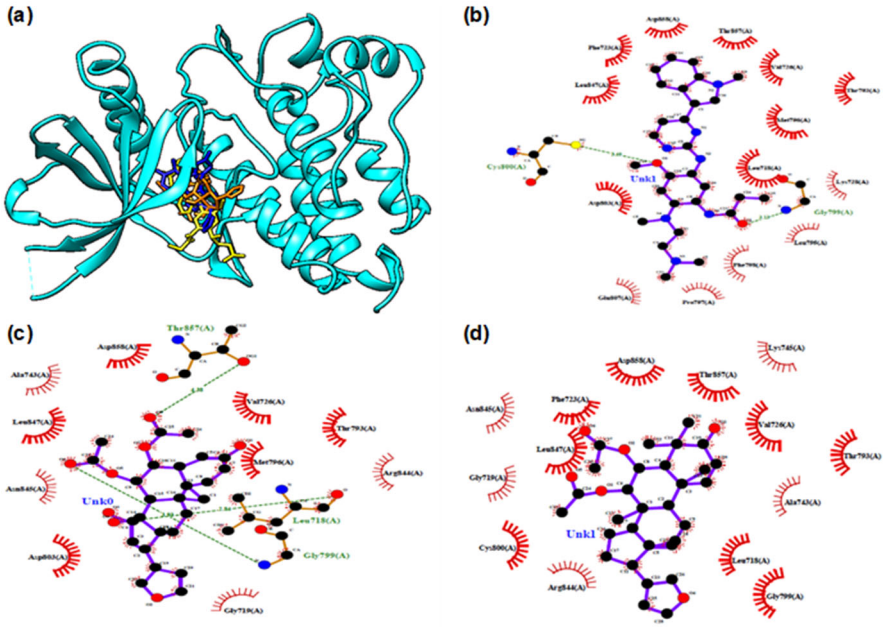

Fig 6. Binding visualization of ligand on EGFR: (a) 3-dimensional visualization of native ligand (yellow), Dysobinol (orange) and dysobinin (blue), (b) native ligand interaction with EGFR, (c) Dysobinol interaction with EGFR, and (d) dysobinin interaction with EGFR

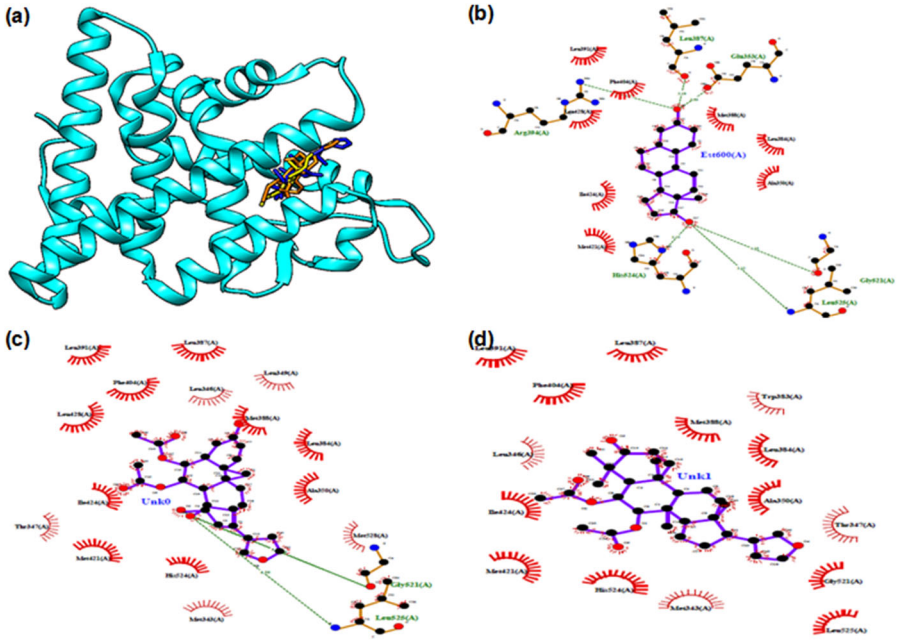

Fig 7. Binding visualization of ligand on mutant ERα: (a) 3-dimensional visualization of native ligand (yellow), Dysobinol (orange) and dysobinin (blue), (b) native ligand interaction with mutant ERα, (c) Dysobinol interaction with mutant ERα, and (d) dysobinin interaction with mutant ERα

toward AKT (−8.2 kcal/mol), comparable to dysobinin (−8.2 kcal/mol), suggesting that AKT may represent a potential molecular target mediating its cytostatic activity. Both compounds also exhibited moderate binding to CDK6, consistent with the observed G1-phase arrest and downregulation of Cyclin D1.

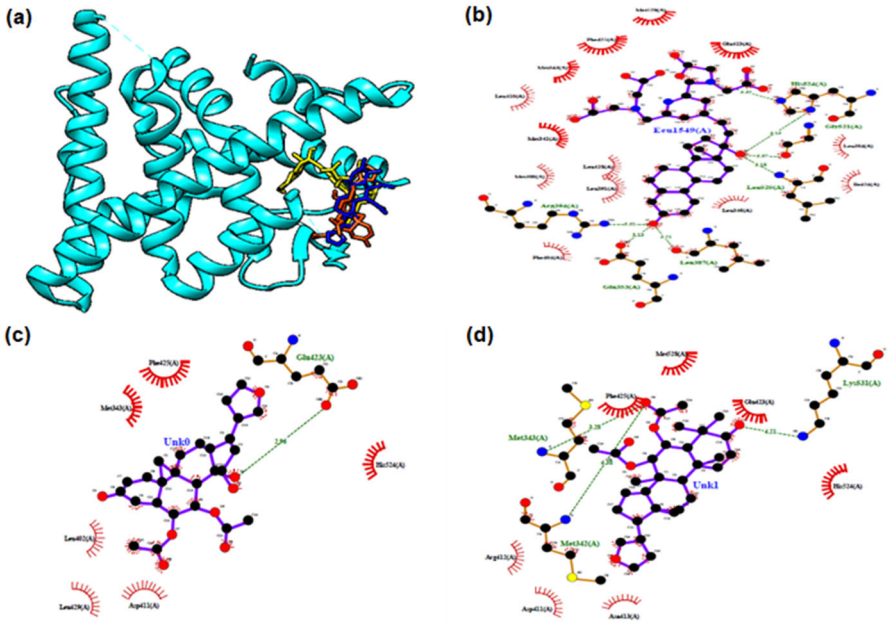

Fig 8. Binding visualization of ligand on Erα rbd: (a) 3-dimensional visualization of native ligand (yellow), Dysobinol (orange) and dysobinin (blue), (b) native ligand interaction with Erα rbd, (c) Dysobinol interaction with Erα rbd, and (d) dysobinin interaction with Erα rbd

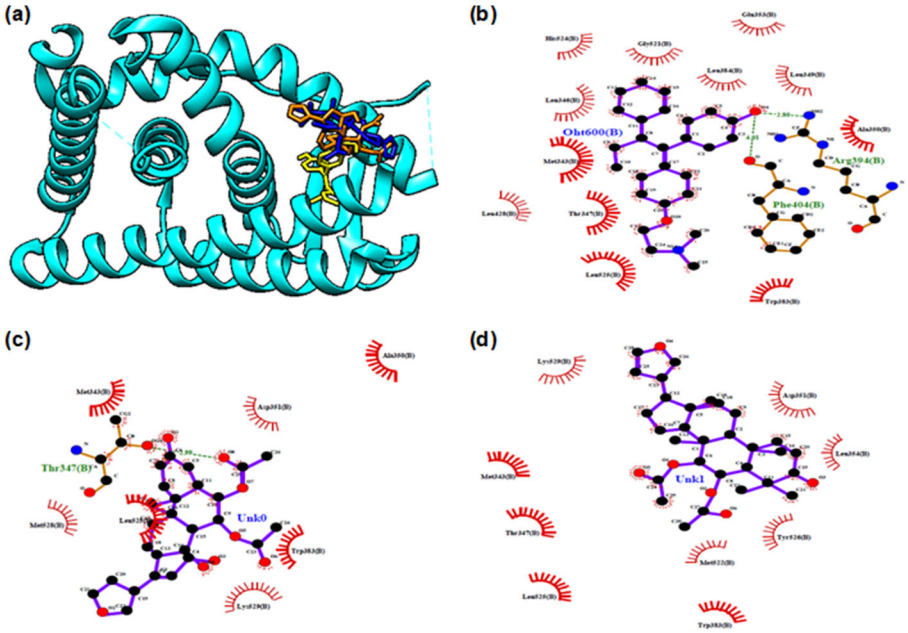

Fig 9. Binding visualization of ligand on ERα ligand-binding domain: (a) 3-dimensional visualization of native ligand (yellow), Dysobinol (orange) and dysobinin (blue), (b) native ligand interaction with ERα ligand-binding domain, (c) Dysobinol interaction with ERα ligand-binding domain, and (d) dysobinin interaction with ERα ligand-binding domain

In contrast, Dysobinol displayed weak or unfavorable binding to VEGFR-1 and VEGFR-2, indicating limited antiangiogenic potential. Binding to estrogen receptor isoforms (mutant ERα and ERα domains) was weaker than native ligands but still notable, suggesting possible interactions relevant to breast cancer cell signaling. Although dysobinin generally exhibited slightly stronger binding than

Dysobinol across most targets, the comparable interaction of Dysobinol with AKT and CDK6 provides a plausible mechanistic link to its observed effects on MCF-7 cell cycle regulation. Further interaction analysis revealed five hydrogen bonds involved in the interaction of Dysobinol with AKT (with Lys276, Asn279, and Gly294) (Fig. 5), and two hydrogen bonds with EGFR (with Leu728 and Gly799) (Fig. 6).

EGFR plays a significant role in the CDK 4/6-cyclin D complex. The arrest of the G1 phase in the cell cycle is the most common result of EGFR inhibition before DNA synthesis [49]. The estrogen receptor α (ERα) is a target that inhibits the progression of the G1 cell cycle since blocking ERα causes the downregulation of cyclin D1 and leads to G1 arrest [50]. Through transcriptional control of cell cycle proteins and a decrease in cell cycle inhibitors, the PI3K/Akt pathway also controls the G1/S cell cycle transition [51]. Inhibition of proteins involved in the cell cycle, such as CDK6, induces G1 arrest [52].

Dysobinol (Fig. 11) shares strong structural similarity with dysobinin from *C. siamensis*, which shows potent cytotoxicity against MCF-7 cells (IC_{50} = 2.15 µg/mL) [31]. However, Dysobinol displayed much lower activity (IC_{50} = 148.20 µg/mL). The key structural differences include the presence of an acetyl group on the B-ring, a methylene group at C-16, and two hydroxyl groups on the D-ring (C-14 and C-15), whereas dysobinin possesses a double bond on the D-ring. These modifications may influence molecular interactions with cellular targets: the additional hydroxyl groups in Dysobinol could increase polarity and reduce membrane permeability or hydrophobic binding, while the absence of the D-ring double bond may alter conformational rigidity and decrease binding affinity [47]. Together, these structural changes likely explain the reduced anticancer activity of Dysobinol compared with dysobinin.

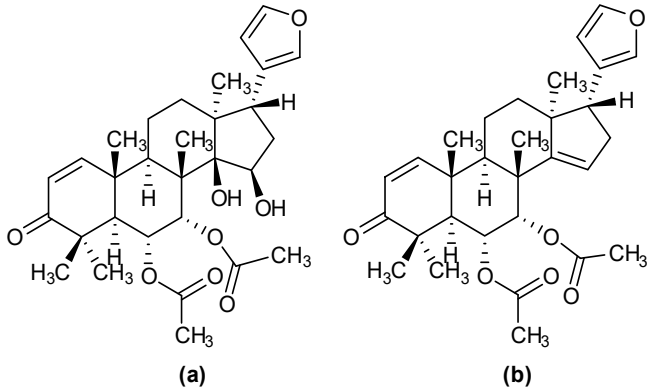

Fig 11. Structures of (a) Dysobinol and (b) dysobinin

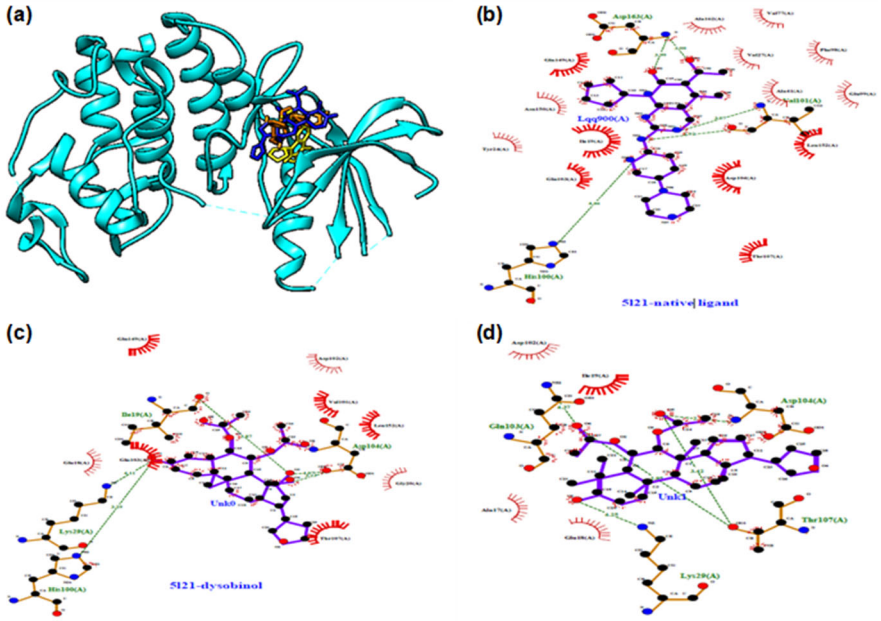

Fig 10. Binding visualization of ligand on CDK6: (a) 3-dimensional visualization of native ligand (yellow), Dysobinol (orange) and dysobinin (blue), (b) native ligand interaction with CDK6, (c) Dysobinol interaction with CDK6, (d) dysobinin interaction with CDK6

Furthermore, Dysobinol inhibits the cell cycle, which could inhibit cell growth/cell proliferation without inducing apoptosis. A similar phenomenon has also been observed for several other anticancer agents [53-54]. Such an agent is expected to avoid toxic side effects in normal cells/tissues. Therefore, Dysobinol could be an effective cytostatic anticancer agent. These findings are consistent with the qPCR data, which demonstrated reduced cyclin D1 expression. As cyclin D1 downregulation can suppress the G1–S phase transition, Dysobinol appears to exert a cytostatic effect by limiting cell cycle progression rather than inducing apoptosis. The concurrent increase in Bcl-2 expression and lack of apoptotic features in flow cytometry further support this mechanism. Collectively, these results suggest that Dysobinol may function as a cell cycle–modulating agent, highlighting its potential as a cytostatic compound for anticancer therapy.

Cyclin D1 plays a pivotal role in controlling the G1–S phase transition by activating CDK4/6 and inactivating the retinoblastoma (Rb) protein, thereby enabling E2F-dependent transcription of genes required for DNA synthesis [49,55-57]. The inhibition of cyclin D1-CDK4/6 mainly causes the G1 phase delay. Prolonged arrest of G1 negatively regulates the replisome component, leading to DNA replication failure and cell cycle exit in a p53-dependent manner [57]. In the present study, the observed downregulation of cyclin D1 following Dysobinol treatment suggests a disruption of this regulatory pathway, consistent with inhibition of cell cycle progression rather than induction of apoptosis. This cytostatic effect positions Dysobinol as a promising lead compound for further development as an anticancer agent targeting cell cycle regulation. Beyond its role in driving the G1–S phase transition, cyclin D1 also modulates signaling pathways that regulate growth, differentiation, and migration, thereby influencing multiple aspects of tumor cell behavior. Dysregulation of cyclin D1 is frequently observed in human cancers, where its overexpression promotes uncontrolled proliferation and tumorigenesis, while loss-of-function alterations can disrupt normal cell cycle control [58-59].

According to the Lipinski, Ghose, Veber, Egan, and Muegge criteria, Dysobinol meets the requirements for a drug-like molecule with no violations. Its favorable bioavailability and Csp^3 scores suggest good oral absorption, which is further supported by pharmacokinetic predictions showing high GI uptake. Dysobinol also exhibits low BBB penetration, a desirable property for minimizing central nervous system (CNS)-related side effects, along with moderate skin permeability (log Kp). In addition, its moderate synthetic accessibility score indicates that structural modification and large-scale synthesis are feasible. Collectively, these features strengthen the potential of Dysobinol as a promising natural product–derived lead compound for anticancer drug development [60]. Dysobinol generally showed slightly reduced docking scores across most targets than dysobinin. This difference can be explained by structural variations: Dysobinol possesses two hydroxyl groups on the D-ring and lacks a double bond present in dysobinin, which likely affects hydrophobic interactions and reduces binding affinity at certain active sites. In contrast, the double bond in dysobinin may stabilize ligand–receptor interactions, contributing to stronger affinities. Despite this, Dysobinol's comparable affinity for AKT and CDK6 highlights these proteins as plausible molecular targets underlying its observed cell cycle inhibitory effects.

■ CONCLUSION

Dysobinol demonstrated cytotoxic activity against the MCF-7 cell line, with evidence of moderate anticancer potential. Mechanistic studies indicate that its effect is primarily cytostatic, inducing G1 cell cycle arrest as reflected by inhibition of DNA synthesis in the S phase and downregulation of cyclin D1, without triggering apoptosis. Such a phenotype is consistent with anticancer agents that minimize toxicity to normal tissues by targeting cell cycle progression. Molecular docking further supported this mechanism, suggesting potential interactions with EGFR, AKT, and cyclin D1. In addition, pharmacokinetic predictions revealed favorable oral bioavailability, limited BBB penetration, and moderate synthetic accessibility, underscoring its promise as a natural product–derived lead compound. Taken together, these findings highlight dysobinol as a

candidate for further *in vivo* validation and potential development as a cytostatic anticancer agent.

■ ACKNOWLEDGMENTS

We would like to acknowledge the financial support provided for this research by the Fundamental Research Grant from the Ministry of Education, Culture, Research, and Technology, Indonesia (148/E5/PG.02.00.PL /2023).

■ CONFLICT OF INTEREST

The authors declare that they have no known competing financial interests or personal relationships that could have appeared to influence the work reported in this paper.

■ AUTHOR CONTRIBUTIONS

Shabarni Gaffar: conceptualization, supervision, writing-review & editing, funding acquisition; Ghina Uli Felicia Tambunan: formal analysis, data curation, writing original draft; Ersanda Hafiz: formal analysis, validation; Tati Herlina: resource, investigation; Hesti Lina Wiraswati: writing-review & editing; Nurlelasari: resources, project administration; Ilma Fauziah Ma'ruf: software, validation, visualization, writing-review & editing.

■ REFERENCES

[1] Centers for Disease Control and Prevention, 2024, *Deaths and Mortality*, https://www.cdc.gov/nchs/fastats/deaths.htm, accessed on 25 August 2024.

[2] Chakraborty, P., 2018, Herbal genomics as tools for dissecting new metabolic pathways of unexplored medicinal plants and drug discovery, *Biochim. Open*, 6, 9–16.

[3] Li, C.Q., Lei, H.M., Hu, Q.Y., Li, G.H., and Zhao, P.J., 2021, Recent advances in the synthetic biology of natural drugs, *Front. Bioeng. Biotechnol.*, 9, 691152.

[4] Wiraswati H.L., Fauziah, N., Pradini, G.W., Kurnia, D., Kodir, R.A., Berbudi, A., Arimdayu, A.R., Laelalugina, A., Supandi, S., and Ma'ruf, I.F., 2023, *Breynia cernua*: Chemical profiling of volatile compounds in the stem extract and its antioxidant, antibacterial, antiplasmodial and anticancer activity *in vitro* and *in silico*, *Metabolites*, 13 (2), 281.

[5] Gezici, S., and Şekeroğlu, N., 2019, Current perspectives in the application of medicinal plants against cancer: Novel therapeutic agents, *Anticancer Agents Med. Chem.*, 19 (1), 101–111.

[6] Azzam, M.H., Fauziah, N., and Wiraswati, H.L., 2022, The anticancer effect of phytochemicals and potential of *Breynia cernua*: An overview, *Biomed. Pharmacol. J.*, 15 (4), 2259–2278.

[7] Greenwell, M., and Rahman, P.K., 2015, Medicinal plants: Their use in anticancer treatment, *Int. J. Pharm. Sci. Res.*, 6 (10), 4103–4112.

[8] Barbuti, A.M., and Chen, Z.S., 2015, Paclitaxel through the ages of anticancer therapy: Exploring its role in chemo-resistance and radiation therapy, *Cancers*, 7 (4), 2360–2371.

[9] Xu, X.H., Li, T., Fong, C.M., Chen, X., Chen, X.J., Wang, Y.T., Huang, M.Q., and Lu, J.J., 2016, Saponins from Chinese medicines as anticancer agents, *Molecules*, 21 (10), 1326.

[10] Faizan, S., Mohammed Abdo Mohsen, M., Amarakanth, C., Justin, A., Ravishankar Rahangdale, R., Raghu Chandrashekar, H., and Prashantha Kumar, B.R., 2024, Quinone scaffolds as potential therapeutic anticancer agents: Chemistry, mechanism of actions, structure-activity relationships and future perspectives, *Res. Chem.*, 7, 101432.

[11] Cai, Y., Zhang, J., Chen, N.G., Shi, Z., Qiu, J., He, C., and Chen, M., 2017, Recent advances in anticancer activities and drug delivery systems of tannins, *Med. Res. Rev.*, 37 (4), 665–701.

[12] Kamran, S., Sinniah, A., Abdulghani, M.A.M., and Alshawsh, M.A., 2022, Therapeutic potential of certain terpenoids as anticancer agents: A scoping review, *Cancers*, 14 (5), 1100.

[13] Shilpi, J.A., Saha, S., Chong, S.L., Nahar, L., Sarker, S.D., and Awang, K., 2016, Advances in chemistry and bioactivity of the genus *Chisocheton* Blume, *Chem. Biodiversity*, 13 (5), 483–503.

[14] Zhang, Y., and Xu, H., 2017, Recent progress in the chemistry and biology of limonoids, *RSC Adv.*, 7 (56), 35191–35220.

[15] Chen, J., Fan, X., Zhu, J., Song, L., Li, Z., Lin, F., Yu, R., Xu, H., and Zi, J., 2018, Limonoids from seeds of

Azadirachta indica A. Juss. and their cytotoxic activity, *Acta Pharm. Sin. B*, 8 (4), 639–644.

[16] Katja, D.G., Farabi, K., Nuraini, V.A., Nurlelasari, N., Hidayat, A.T., Mayanti, T., Harneti, D., and Supratman, U., 2016, A New 30-nor trijugin-type limonoid, chisotrijugin, from the bark of *Chisocheton cumingianus* (Meliaceae), *Int. J. Chem.*, 8 (3), 30–34.

[17] Supratman, U., Salam, S., Naibaho, W., Fajar, M., Nurlelasari, N., Katja, D.G., Harneti, D., Maharani, R., Hidayat, A.T., Lesmana, R., Azlan Nafiah, M., and Shiono, Y., 2020, New cytotoxic limonoids from the stem bark of *Chisocheton pentandrus* (Blanco) Merr, *Phytochem. Lett.*, 35, 63–67.

[18] Harneti, D., Salam, S., Nurlelasari, N., Maharani, R., Mayanti, T., Safari, A., Hidayat, A.T., Lesmana, R., Fajriah, S., Supratman, U., Prescott, T., Shiono, Y., 2023, Pentandricines F-H, cytotoxic limonoids from the stem bark of *Chisocheton pentandrus* (Blanco) Merr, *Phytochem. Lett.*, 54, 119–124.

[19] Mohamad, K., Hirasawa, Y., Litaudon, M., Awang, K., Hadi, A.H.A., Takeya, K., Ekasari W., Widyawaruyanti, A., Zaini, N.C., and Morita, H., 2009, Ceramicines B–D, new antiplasmodial limonoids from *Chisocheton ceramicus*, *Bioorg. Med. Chem.*, 17 (2), 727–30.

[20] Phongmaykin, J., Kumamoto, T., Ishikawa, T., Suttisri, R., and Saifah, E., 2008, A new sesquiterpene and other terpenoid constituents of *Chisocheton penduliflorus*, *Arch. Pharmacal Res.*, 31 (1), 21–27.

[21] Tasyriq, M., Najmuldeen, I.A., In, L.L., Mohamad, K., Awang, K., and Hasima, N., 2012, 7α-Hydroxy-β-sitosterol from *Chisocheton tomentosus* induces apoptosis via dysregulation of cellular Bax/Bcl-2 ratio and cell cycle arrest by downregulating ERK1/2 activation, *Evidence-Based Complementary Altern. Med.*, 2012 (1), 765316.

[22] Inada, A., Somekawa, M., Murata, H., Nakanishi, T., Tokuda, H., Nishino, H., Iwashima, A., Darnaedi, D., and Murata, J., 1993, Phytochemical studies on Meliaceous plants. VIII. Structures and inhibitory effects on Epstein-Barr virus activation of triterpenoids from leaves of *Chisocheton macrophyllus* King, *Chem. Pharm. Bull.*, 41 (3), 617–619.

[23] Yang, M.H., Wang, J.S., Luo, J.G., Wang, X.B., and Kong, L.Y., 2011, Chisopanins A–K, 11 new protolimonoids from *Chisocheton paniculatus* and their anti-inflammatory activities, *Bioorg. Med. Chem.*, 19 (4), 1409–1417.

[24] Chan, K.Y., Mohamad, K, Ooi A.J.A., Imiyabir, Z., and Chung, L.Y., 2012, Bioactivity-guided fractionation of the lipoxygenase and cyclooxygenase inhibiting constituents from *Chisocheton polyandrus* Merr, *Fitoterapia*, 83 (5), 961–967.

[25] Hoai, N.T., Duc, H.V., Raal, A., and Morita, H., 2018, A new limonoid from *Chisocheton paniculatus* fruit collected in Vietnam and its NO production inhibitory activity, *Nat. Prod. Commun.*, 13 (10), 1255–1257.

[26] Bailly, C., 2024, Limonoids isolated from *Chisocheton ceramicus* Miq. and the antiadipogenic mechanism of action of ceramicine B, *Arch Pharm.*, 357 (8), 2400160.

[27] Chong, S.L., Hematpoor, A., Hazni, H., Sofian-Azirun, M., Litaudon, M, Supratman, U., Murata, M., and Awang, K., 2019, Mosquito larvicidal limonoids from the fruits of *Chisocheton erythrocarpus* Hiern, *Phytochem. Lett.*, 30, 69–73.

[28] Álvarez-Caballero, J.M., and Coy-Barrera, E., 2019, Chemical and antifungal variability of several accessions of *Azadirachta indica* A. Juss. from six locations across the Colombian Caribbean coast: Identification of antifungal azadirone limonoids, *Plants*, 8 (12), 555.

[29] Nurlelasari, N., Katja, D.G., Harneti, D., Wardayo, M.M., Supratman, U., and Awang, K., 2017, Limonoids from the seeds of *Chisocheton macrophyllus*, *Chem. Nat. Compd.*, 53 (1), 83–87.

[30] Maneerat, W., Laphookhieo S., Koysomboon, S., and Chantrapromma K., 2008, Antimalarial, antimycobacterial and cytotoxic limonoids from *Chisocheton siamensis*, *Phytomedicine*, 15 (12), 1130–1134.

[31] Wong, C.P., Shimada, M., Nagakura, Y., Nogroho, A.E., Hirasawa, Y., Kaneda, T., Awang, K., Hadi, A.H.A., Mohamad, K., Shiro, M., and Morita, H.,

2011, Ceramicines E—I, new limonoids from *Chisocheton ceramicus*, *Chem. Pharm. Bull.*, 59 (3), 407–411.

[32] Supriatno, S., Nurlelasari, N., Herlina, T, Harneti, D., Maharani R., Hidayat, A.T., Mayanti, T., Supratman, U., Azmi M.N., and Shiono, Y., 2018, A new limonoid from stem bark of *Chisocheton pentandrus* (Meliaceae), *Nat. Prod. Res.*, 32 (21), 2610–2616.

[33] Pettit, G.R., Barton, D.H.R., Herald, C.L., Polonsky, J, Schmidt, J.M., and Connolly, J.D., 1983, Evaluation of limonoids against the murine P388 lymphocytic leukemia cell line, *J. Nat. Prod.*, 46 (3), 379–390.

[34] Luo, X., Yu, Z., Yue, B., Ren, J., Zhang, J., Mani, S., Wang, Z., and Dou, W., 2020, Obacunone reduces inflammatory signalling and tumour occurrence in mice with chronic inflammation-induced colorectal cancer, *Pharm. Biol.*, 58 (1), 886–897.

[35] Nivetha, R., Arvindh, S., Baba, A.B., Gade, D.R., Gopal, G., Chitrathara, K., Reddy, K.P., Reddy, G.B., and Nagini, S., 2022, Nimbolide, a neem limonoid, inhibits angiogenesis in breast cancer by abrogating aldose reductase mediated IGF-1/PI3K/Akt signalling, *Anti-Cancer Agents Med. Chem.*, 22 (14), 2619–2636.

[36] Yang, T., Wu, E., Zhu, X., Leng, Y., Ye, S., Dong, R., Liu, J., Zhong, J., Zheng, Y., Xu, W., Luo, J., Kong, L., and Zhang, H., 2022, TKF, a mexicanolide-type limonoid derivative, suppressed hepatic stellate cells activation and liver fibrosis through inhibition of the YAP/Notch3 pathway, *Phytomedicine*, 107, 154466.

[37] Chandel, S., Bhattacharya, A., Gautam, A., Zeng, W., Alka, O., Sachsenberg, T., Gupta, G.D., Narang, R.K., Ravichandiran, V., and Singh, R., 2024, Investigation of the anti-cancer potential of epoxyazadiradione in neuroblastoma: Experimental assays and molecular analysis, *J. Biomol. Struct. Dyn.*, 42 (21), 11377–11395.

[38] Shi, Y.S., Zhang, Y., Li, H.T., Wu, C.H., El-Seedi, H.R., Ye, W.K., Wang, Z.W., Li, C.B., Zhang, X.F., and Kai, G.Y., 2020, Limonoids from *Citrus*: Chemistry, anti-tumor potential, and other bioactivities, *J. Funct. Foods*, 75, 104213.

[39] Obeagu, E.I., and Obeagu, G.U., 2024, Breast cancer: A review of risk factors and diagnosis, *Medicine*, 103 (3), e36905.

[40] Anwar, S.L., Raharjo, C.A., Herviastuti, R., Dwianingsih, E.K., Setyoheriyanto, D., Avanti, W.S., Choridah, L., Harahap, W.A., Darwito, D., Aryandono, T., and Wulaningsih, W., 2019, Pathological profiles and clinical management challenges of breast cancer emerging in young women in Indonesia: a hospital-based study, *BMC Women's Health*, 19 (1), 28.

[41] Livak, K.J., and Schmittgen, T.D., 2001, Analysis of relative gene expression data using real-time quantitative PCR and the $2^{-\Delta\Delta C_T}$ method, *Methods*, 25 (4), 402–408.

[42] Daina, A., Michielin, O., and Zoete, V., 2017, SwissADME: A free web tool to evaluate pharmacokinetics, drug-likeness and medicinal chemistry friendliness of small molecules, *Sci. Rep.*, 7 (1), 42717.

[43] Eberhardt, J., Santos-Martins, D., Tillack, A.F., and Forli, S., 2021, AutoDock Vina 1.2.0: New docking methods, expanded force field, and python bindings, *J. Chem. Inf. Model.*, 61 (8), 3891–3898.

[44] Pettersen, E.F., Goddard, T.D., Huang, C.C., Meng, E.C., Couch, G.S., Croll, T.I., Morris, J.H., and Ferrin, T.E., 2021, UCSF ChimeraX: Structure visualization for researchers, educators, and developers, *Protein Sci.*, 30 (1), 70–82.

[45] Laskowski, R.A., and Swindells, M.B., 2011, LigPlot+: Multiple ligand–protein interaction diagrams for drug discovery, *J. Chem. Inf. Model.*, 51 (10), 2778–2786.

[46] Youssef, A.M.M., Maaty, D.A.M., and Al-Saraireh, Y.M., 2023, Phytochemistry and anticancer effects of Mangrove (*Rhizophora mucronata* Lam.) leaves and stems extract against different cancer cell lines, *Pharmaceuticals*, 16 (1), 4.

[47] Nagulapalli Venkata, K.C., Rathinavelu, A., Bishayee, A., 2018, Limonoids: Structure–activity relationship studies and anticancer properties, *Stud. Nat. Prod. Chem.*, 59, 375–399.

[48] Crowley, L.C., Marfell, B.J., Scott, A.P., and Waterhouse, N.J., 2016, Quantitation of apoptosis and necrosis by Annexin V binding, propidium iodide uptake, and flow cytometry, *Cold Spring Harb Protoc*., 2016 (11), pdb.prot087288.

[49] Crozier, L., Foy, R., Mouery, B., Whitaker, R., Corno, A., Spanos, C., Ly, T., Gowen Cook, J., and Saurin, A.T., 2022, CDK4/6 inhibitors induce replication stress to cause long-term cell cycle withdrawal, *The EMBO J.*, 41 (6), e108599.

[50] Elshal, M., Eid, N., El-Sayed, I., El-Sayed, W., and Al-Karmalawy, A., 2021, Concanavalin-A shows synergistic cytotoxicity with tamoxifen via inducing apoptosis in estrogen receptor-positive breast cancer: *In vitro* and molecular docking studies, *Pharm. Sci.*, 28 (1), 75–85.

[51] Huang, T.T., Lampert, E.J., Coots, C., and Lee, J.M., 2020, Targeting the PI3K pathway and DNA damage response as a therapeutic strategy in ovarian cancer, *Cancer Treat. Rev.*, 86, 102021.

[52] Saleban, M., Harris, E.L., and Poulter, J.A., 2023, D-type cyclins in development and disease, *Genes*, 14 (7), 1445.

[53] Morley, K.L., Ferguson, P.J., and Koropatnick, J., 2007, Tangeretin and nobiletin induce G1 cell cycle arrest but not apoptosis in human breast and colon cancer cells, *Cancer Lett.*, 251 (1), 168–178.

[54] Kaku, Y., Tsuchiya, A., Kanno, T., and Nishizaki, T., 2015, Irinotecan induces cell cycle arrest, but not apoptosis or necrosis, in Caco-2 and CW2 colorectal cancer cell lines, *Pharmacology*, 95 (3-4), 154–159.

[55] Topacio, B.R., Zatulovskiy, E., Cristea, S., Xie, S., Tambo, C.S., Rubin, S.M., Sage, J., Kõivomägi, M., and Skotheim, J.M., 2019, Cyclin D-Cdk4,6 drives cell-cycle progression via the retinoblastoma protein's C-terminal helix, *Mol. Cell*, 74 (4), 758–770.e4.

[56] Qie, S., and Diehl, J.A., 2016, Cyclin D1, cancer progression, and opportunities in cancer treatment, *J. Mol. Med.*, 94 (12), 1313–1326.

[57] Yang, Y., Wu, J., Cai, J., He, Z., Yuan, J., Zhu, X., Li, Y., Li, M., and Guan, H., 2015, PSAT1 regulates cyclin D1 degradation and sustains proliferation of non-small cell lung cancer cells, *Int. J. Cancer*, 136 (4), E39–E50.

[58] Abbas, S.E., George, R.F., Samir, E.M., Aref, M.M., and Abdel-Aziz, H.A., 2019, Synthesis and anticancer activity of some pyrido[2,3-*d*] pyrimidine derivatives as apoptosis inducers and cyclin-dependent kinase inhibitors, *Future Med. Chem.*, 11 (18), 2395–2414.

[59] Wee, P., and Wang, Z., 2017, Epidermal growth factor receptor cell proliferation signaling pathways, *Cancers*, 9 (5), 52.

[60] Michalak, O., Cybulski, M., Szymanowski, W., Gornowicz, A., Kubiszewski, M., Ostrowska, K., Krzeczyński, P., Bielawski, K., Trzaskowski, B., and Bielawska, A., 2023, Synthesis, biological activity, ADME and molecular docking studies of novel ursolic acid derivatives as potent anticancer agents, *Int. J. Mol. Sci.*, 24 (10), 8875.